

A UNIFIED FAST SOLUTION FOR THE SINGLE/ INTERFEROMETER/STEREO SAR GEOLOCATION EQUATION BASED ON THE RDPC MODEL

Haifeng Huang^{*} and Qingsong Wang

School of Electronic Science and Engineering, National University of Defense Technology, Changsha, Hunan 410073, P. R. China

Abstract—The model based on range and Doppler equations (RD model) is the most precise model for SAR geolocation, and therefore SAR geolocation based on this RD model has become more and more popular. Unfortunately, the RD method requires iterative solution, in most case, which is time-consuming and prone to poor optimization due to observation errors of parameters. In face of the huge mass of measured data from global SAR measurements, how to improve processing speed while maintaining geolocation accuracy is an important problem. This paper examines how to solve the RD geolocation equations for single, interferometric, and stereo SAR. First, the RD geolocation equations for the three kinds of systems are abstracted into a unified equation form. Second, it is determined that the RD geolocation equation can be approximated as a mapping relationship using polynomials. Then a fast solution method for the unified geolocation equation is proposed based on the Range Doppler Polynomial Coefficient Model (RDPC). Third, the accuracy loss of the RDPC model is analyzed, and the precision differences among the three kinds of system are compared. Finally, several groups of TerraSAR-X measured data for the three modes are processed using the fast algorithm. The results show that the fast algorithm greatly reduces the amount of calculation while the geolocation accuracy loss is small. Performance evaluation demonstrates that the proposed method is efficient and correct.

Received 1 May 2013, Accepted 22 June 2013, Scheduled 5 July 2013

* Corresponding author: Haifeng Huang (h.haifeng@163.com).

1. INTRODUCTION

With the development of synthetic aperture radar technology, spaceborne SAR has become one of the main means of high-precision geolocation [1–3]. Spaceborne SAR geolocation technology includes three modes: single SAR image geolocation [4], interferometric SAR geolocation [5], and stereo SAR geolocation [6]. It exists simultaneously in these three kinds of modes that one has to solve the geolocation equations. The model based on range and Doppler equations (the RD model) is the most precise model for SAR geolocation and therefore has become more and more popular. Unfortunately, in most case, the RD method requires iterative solution, which is time-consuming and prone to poor optimization due to observation errors of parameters and seriously depends on initial value [7, 8]. For example, the distributed small satellites synthetic aperture radar (DSS-SAR) geolocation is based on non-linear equation and iterative solution is required. The observation errors of parameters include errors on satellite position, velocity, baseline, phase, etc.. These errors will slow iterative process and even the iterative process does not converge [1, 5, 9].

Until now, global SAR measurements have accumulated a large mass of data. For example, it has taken nearly two years to finish global data processing for the SRTM task, for which the total volume of global data is approximately 9.8 TB. In addition, the German Aerospace Center (DLR) is currently using two TerraSAR-X and TanDEM-X satellites to set up an interferometric measuring system in which they fly in formation [5, 10]. The system is expected to complete global DEM measurements meeting HRTI-3 standard in three years and to obtain an amount of data greater than 350 TB. In face of this huge mass of data from global SAR measurements, how to improve processing speed while maintaining geolocation accuracy is a problem which deserves to be taken into account.

The synthetic aperture radar imaging process essentially involves performing a three-dimensional ground-point projection onto a 2D image plane. In other words, it establishes a mapping relationship between each object point and an image point. All kinds of SAR geolocation technology are based on this mapping relation. At present, three main models are used to describe the mapping relation model.

The first class of model is the equivalent-line central-projection models based on photogrammetry theory. There are two types of these models; the first one was proposed by Leberl [4, 11, 12]. Changes of linear elements in the sensor's exterior azimuthal elements are considered, but not angle elements. Therefore, an SAR stereo model

constructed on this basis experiences moderately large fluctuations in parallax, as is also the case with airborne SAR because this model is built in terms of the range equation of image points and the zero Doppler condition. The second type is the mathematical model of flat-range projective radar images proposed by Konecny and Schuhu [13]. In this model, changes in the exterior azimuthal elements of sensors and terrain are considered, and the form of the equation is similar to the photogrammetric collinearity equation. Although the model is easy to use, it interprets an object with reference only to the characteristics of traditional optical imaging, without taking into account the side-looking projective characteristics of an SAR image. For this reason, this type of model is used only as a simulation processing method for optical images.

The second class of model is the RPC (Rational Polynomial Coefficient) model. This model associates each ground-point coordinate with its corresponding image-point coordinate using a ratio of polynomials. Use of this model to replace the space optical model has been generally accepted [14]. Zhang et al. [15] recently applied this model to SAR geolocation. The main difficulty of the method is the need to solve a large system of linear equations to compute the parameters of the RPC model.

The third class of model is the RD (Range Doppler) model, proposed by Brown [16] and Curlander [17], which contains two equations: the range equation and the Doppler equation. The model fully reflects the two-dimensional nature of SAR imaging. The range equation describes the distance relationship between the radar and the object point after pulse compression. The Doppler equation describes the Doppler relationship between the radar and the object point at the moment of azimuth focusing.

Because the RD model is characterized by rigor and high accuracy, it is the most widely used. Single SAR image geolocation is implemented through simultaneous equations, including earth-model equations and RD equations. These equations do not have an analytic solution, and therefore solving for the object-point position requires complex iterative computations, so efficiency is low. Many scholars have investigated this problem, including the extraction and optimization of model parameters, coordinate transformations, positioning error source analysis, and other aspects of the problem [18–21]. Many international scientific research institutions, such as JPL, DLR, and the Italian space agency, have developed their own SAR image geolocation processing modules based on the RD model. The RD model is also widely used in stereo SAR geolocation technology, in which the system of simultaneous equations includes the two Doppler

equations and the two range equations of the two images. The method also requires complex iterative calculations [6, 22]. Similarly, InSAR geolocation technology has also widely adopted the RD model. Various forms of geolocation methods have been proposed based on the RD model. To address the complexity of the iterative computations, many researchers have proposed various approximation methods to improve computational efficiency. Studies in the literature [23–25] have investigated DEM reconstruction under the hypothesis of a flat ground and side-looking radar, which entails a large reconstruction error. A closed-form solution based on range spheres, Doppler cones, and a phase hyperboloid has been presented in [26, 27]. However, the deduction is based on monostatic equation hypothesis in that case. For the bistatic equation case, such as SRTM and TanDEM-X mission, a closed-form solution cannot be derived. The Integrated TanDEM-X Processor [28, 29], a fast and efficient technique for SAR interferogram geocoding which uses object-to-image transformation, is also based on the RD model.

This paper examines how to solve the RD geolocation equations rapidly for single, interferometric, and stereo SAR and is organized as follows. The RD geolocation equations for the three kinds of system are abstracted into a unified equation form in Section 2. Based on proposals in the literature [30], a fast solution for the unified geolocation equation is proposed in Section 3. Section 4 analyzes the accuracy loss of the RDPC model and presents a comparison of the differences in precision among the three models. To verify the effectiveness of this method, the results of processing real TerraSAR-X data were used in Section 5, and conclusions are drawn in the final section.

2. UNIFIED RD GEOLOCATION EQUATIONS

Let O_e - XYZ be an Earth fixed-coordinate system, \mathbf{S}_1 the spatial vector for the first satellite, \mathbf{S}_2 the spatial vector for the second satellite, and \mathbf{P} the spatial location of the ground-target point vector. The Spatial geometry of Earth fixed-coordinate system is shown in Figure 1. The geolocation equations for single, stereo, and interferometric SAR can be abstracted into a unified geolocation equation form as follows:

First range equation (master image range equation):

$$r_1 = |\mathbf{P} - \mathbf{S}_1| \quad (1)$$

Master image Doppler equation:

$$\mathbf{V}_1 \cdot (\mathbf{P} - \mathbf{S}_1) = -\frac{\lambda}{2} f_1 r_1 \quad (2)$$

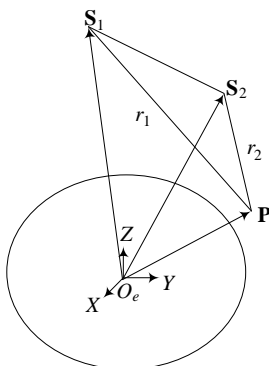


Figure 1. Spatial geometry of Earth fixed-coordinate system.

Second range equation:

$$\frac{(x_2 - x)^2 + (y_2 - y)^2}{A^2} + \frac{(z_2 - z)^2}{B^2} = 1 \tag{3}$$

where r_1 , f_1 , and \mathbf{V}_1 are the slant range, the Doppler centroid, and the velocity vector of the first satellite, and (x, y, z) represents the three-dimensional coordinates of \mathbf{P} . The first two equations for the three kinds of geolocation system are the same, i.e., the first slant-range equation and the Doppler equation of the master image. However, the second slant-range equation has different meanings for all three kinds of geolocation system. In the case of interferometric and stereo SAR geolocation systems, Equation (3) represents the slant-range equation of the target and the second satellite:

$$\mathbf{S}_2 = [x_2, y_2, z_2]^T \tag{4}$$

$$A = B = r_2 = r_1 + \frac{\lambda}{2\pi} \cdot \frac{1}{k} \cdot \phi \quad (\text{for InSAR}) \tag{5}$$

$$A = B = r_2 = r_1 + \Delta r \quad (\text{for stereo SAR}) \tag{6}$$

where r_2 is the slant range of the second satellite, and Δr , ϕ are the differences of the range and the interferometric phase respectively, $k = 2$ for monostatic case and $k = 1$ for bistatic case.

For the case of single SAR geolocation, Equation (3) denotes the slant-range equation for the target and the earth-ellipsoid double focus:

$$[x_2, y_2, z_2]^T = [0, 0, 0]^T \tag{7}$$

$$A = R_e + h, \quad B = R_p \tag{8}$$

where R_e , R_p are Earth's equatorial radius and polar radius respectively and h is the target elevation.

To illustrate the principle of geolocation, the above equations are presented in a simplified form. In fact, there are many complex situations in the actual system. Taking for example the TanDEM-X mission, the second slant-range equation has the form of two radical sign, and a closed-form solution cannot be derived by literature [26, 27]. Therefore the equations require an iterative solution. Therefore, it is necessary to improve the processing speed and to look for a faster processing method.

3. FAST ALGORITHM FOR RD GEOLOCATION EQUATIONS

3.1. The Unified Fast Algorithm Based on RDPC Model

In fact, Equations (1)–(3) represent the mapping relationship between two three-dimensional spaces:

$$\mathbb{F}: (a, r, \xi) \rightarrow (x, y, z) \quad (9)$$

where a , r are the azimuth and range coordinates of the master SAR image, and ξ has a different meaning in all three cases. In the single SAR case, ξ represents the elevation h of the 2D image coordinates (a, r) ; in the InSAR case, ξ represents the interferometric phase ϕ ; and in the stereo SAR case, ξ represents the slant-range difference between the two images. (x, y, z) represents the three-dimensional coordinates $\mathbf{P} = [x, y, z]^T$ of the ground-scattering unit corresponding to pixel (a, r) .

Analysis shows that the mapping relationship described above, under certain approximate conditions, has the following characteristics:

1. When a, r is fixed, the mapping relationship ($\xi \rightarrow \mathbf{P}(\xi) = [x(\xi), y(\xi), z(\xi)]^T$) can be approximated by the order- m polynomial $\mathbf{P}_m(\xi) = [p_x(\xi), p_y(\xi), p_z(\xi)]^T$.

2. In the local area, the spatial variability of the space geometric model is smaller, or in other words, the order- m polynomials $\mathbf{P}_m(\xi)$ have small differences between nearby pixels.

The approximate conditions noted above will be described further in Section 4. Assuming that the above characteristics hold, then rapid geolocation will be possible. Based on these two approximations, the main task of fast geolocation is how to obtain the polynomial expression corresponding to each pixel of the SAR image. The basic concept of the fast algorithm for the unified system of RD equations is given below:

First, calculate the polynomial corresponding to the coarse pixel points of the SAR image. Assume that a, r are independent variables

and that ξ is the function value. After coarse sampling of a, r by a factor of k along the azimuth and a factor of l over the range, superimpose n fixed deviations $\Delta\xi_i$ ($i = 1, 2, \dots, n$) on ξ . A set of parameter vectors $\{a, r, \xi(a, r) + \Delta\xi_i, P = (x_i, y_i, z_i)\}$ ($i = 1, 2, \dots, n$) can be obtained by solving Equations (1)–(3). Then an order- m ($m < n$) polynomial ($p_x(\xi), p_y(\xi), p_z(\xi)$) for each coarse grid point can be constructed.

Second, order- m polynomials ($p_x(\xi), p_y(\xi), p_z(\xi)$) can be computed for every pixel by bilinear interpolation of the coarse grid points.

Finally, the three-dimensional coordinates of every pixel can be computed by substituting the value of ξ into its corresponding polynomial ($p_x(\xi), p_y(\xi), p_z(\xi)$).

3.2. Fast Algorithm for InSAR Geolocation

In the case of InSAR geolocation, ξ represents the interferometric phase ϕ . The fast algorithm can be divided into the following four steps:

Step 1: Resample the absolute phase $\phi(a, r)$, which was generated by unwrapping and by a factor of k along the azimuth and a factor of l over the range to obtain the absolute interferogram $\phi(a_c, r_c)$ for the coarse grid position.

Step 2: Assuming a phase deviation of $\Delta\phi$ (the absolute phase changes to $\phi(a_c, r_c) + \Delta\phi$) for each pixel $\phi(a_c, r_c)$ of the resampled interferogram, a set of parameter vectors $\{a_c, r_c, \phi(a_c, r_c) + \Delta\phi, P = (x, y, z)\}$ can be obtained by solving Equations (1)–(3) and (5). This group of vectors can accurately describe the interferometric mapping geometry of pixel (a_c, r_c) . Taking an order-three polynomial ($n = 4$) as an example, and repeating the procedure for the four different phase deviations ($\Delta\phi_1, \Delta\phi_2, \Delta\phi_3, \Delta\phi_4$) yields their four corresponding groups of geometric parameter vectors, which represent the conversion from the absolute phase to the ground targets $P_i = (x_i, y_i, z_i)$, $i = \{1, 2, 3, 4\}$. From the four groups of geometric parameter vectors, three cubic polynomials ($p_x(\phi), p_y(\phi), p_z(\phi)$) were constructed to describe the dependence of the 3-D coordinates $P = (x, y, z)$ on the absolute phase ϕ . This process can be defined as follows:

$$\begin{aligned}
 & \begin{bmatrix} 1 & \phi(a_c, r_c) + \Delta\phi_1 & (\phi(a_c, r_c) + \Delta\phi_1)^2 & (\phi(a_c, r_c) + \Delta\phi_1)^3 \\ 1 & \phi(a_c, r_c) + \Delta\phi_2 & (\phi(a_c, r_c) + \Delta\phi_2)^2 & (\phi(a_c, r_c) + \Delta\phi_2)^3 \\ 1 & \phi(a_c, r_c) + \Delta\phi_3 & (\phi(a_c, r_c) + \Delta\phi_3)^2 & (\phi(a_c, r_c) + \Delta\phi_3)^3 \\ 1 & \phi(a_c, r_c) + \Delta\phi_4 & (\phi(a_c, r_c) + \Delta\phi_4)^2 & (\phi(a_c, r_c) + \Delta\phi_4)^3 \end{bmatrix} \begin{bmatrix} c_{0x} & c_{0y} & c_{0z} \\ c_{1x} & c_{1y} & c_{1z} \\ c_{2x} & c_{2y} & c_{2z} \\ c_{3x} & c_{3y} & c_{3z} \end{bmatrix} \\
 & = \begin{bmatrix} x_1 & y_1 & z_1 \\ x_2 & y_2 & z_2 \\ x_3 & y_3 & z_3 \\ x_4 & y_4 & z_4 \end{bmatrix} \tag{10}
 \end{aligned}$$

Then

$$p_x(\phi) = c_{0x} + c_{1x}\phi + c_{2x}\phi^2 + c_{3x}\phi^3, \tag{11}$$

$$p_y(\phi) = c_{0y} + c_{1y}\phi + c_{2y}\phi^2 + c_{3y}\phi^3, \tag{12}$$

$$p_z(\phi) = c_{0z} + c_{1z}\phi + c_{2z}\phi^2 + c_{3z}\phi^3. \tag{13}$$

The selection principle for the phase bias of $(\Delta\phi_1, \Delta\phi_2, \Delta\phi_3, \Delta\phi_4)$ as defined above is to take four equal portions of the points in the range of the interferometric phase in a sampling unit, in which there are k pixels in the azimuth direction and l pixels in the range direction. The maximum and minimum values of the interferometric phase can be computed from the four corner points of the sampling unit:

$$\phi_{i \max} = \max(\phi(a_{ci}, r_{cj}), \phi(a_{c(i+1)}, r_{cj}), \phi(a_{ci}, r_{c(j+1)}), \phi(a_{c(i+1)}, r_{c(j+1)})) \tag{14}$$

$$\phi_{i \min} = \min(\phi(a_{ci}, r_{cj}), \phi(a_{c(i+1)}, r_{cj}), \phi(a_{ci}, r_{c(j+1)}), \phi(a_{c(i+1)}, r_{c(j+1)})) \tag{15}$$

wherein i and j are the azimuth and range coordinates of absolute interferogram after coarse sampling in step 1.

Then the phase bias $\Delta\phi_m$ can be computed as follows:

$$\Delta\phi_m = \begin{cases} m \cdot (\phi_{i \max} - \phi_{i \min}) / 4, & \text{if } \phi(a_{ci}, r_{cj}) \leq (\phi_{i \max} + \phi_{i \min}) / 2 \\ -m \cdot (\phi_{i \max} - \phi_{i \min}) / 4, & \text{if } \phi(a_{ci}, r_{cj}) > (\phi_{i \max} + \phi_{i \min}) / 2 \end{cases},$$

$$m = \{1, 2, 3, 4\} \tag{16}$$

Step 3: Once the polynomials for each grid point (a_c, r_c) have been determined, the polynomials $(p'_x(\phi), p'_y(\phi), p'_z(\phi))$ for each sample of the original interferogram can be obtained. For each sample, the polynomials are constructed by applying bilinear interpolation to the polynomials $(p_x(\phi)_j, p_y(\phi)_j, p_z(\phi)_j, j = \{0, 1, 2, 3\})$ from the adjacent resampling grid:

$$p'_x(\phi) = \text{bilinear}([p_x(\phi)_j, j = \{0, 1, 2, 3\}]), \tag{17}$$

$$p'_y(\phi) = \text{bilinear}([p_y(\phi)_j, j = \{0, 1, 2, 3\}]), \tag{18}$$

$$p'_z(\phi) = \text{bilinear}([p_z(\phi)_j, j = \{0, 1, 2, 3\}]). \tag{19}$$

Step 4: For each original interferogram sample (a, r) , the corresponding 3-D coordinates $(x(a, r), y(a, r), z(a, r))$ can be obtained by substituting the absolute interferometric phase $\phi(a, r)$ into Equations (17)–(19):

$$\begin{cases} x(a, r) = p'_x(\phi(a, r)) \\ y(a, r) = p'_y(\phi(a, r)) \\ z(a, r) = p'_z(\phi(a, r)) \end{cases} \tag{20}$$

Note that the iterative method of solving the 3-D equation systems has been replaced by a polynomial approximation, which is much faster to compute.

3.3. Fast Algorithm for Stereo SAR Geolocation

For the case of stereo SAR geolocation, ξ represents the slant-range difference Δr between the two images. Because the slant-range difference Δr and the interferometric phase ϕ differ only by a proportional coefficient, the algorithm steps for stereo SAR geolocation are the same as those for InSAR geolocation. The selection principle for determining the bias of Δr is to take equal portions of the points in the range of Δr in a sampling unit, and in this unit, it can be computed using the range coordinates of the two SAR images.

3.4. Fast Algorithm for Single SAR Geolocation

For the case of single SAR, ξ represents the elevation h of the 2D image coordinates (a, r) . The algorithm steps for single SAR geolocation are similar to those for InSAR geolocation. The selection principle for determining the bias of Δh is to take equal portions of the points in the range of the elevation within a sampling unit. Because of the need for maximum and minimum operations to determine sampling-unit elevation, a large amount of calculation is required. In fact, h_i can be uniformly distributed over the elevation range $(-500 \text{ m}, 9000 \text{ m})$ at various points on the earth. Take a second-order polynomial as an example: $h_1 = -500 \text{ m}$, $h_2 = 4250 \text{ m}$, $h_3 = 9000 \text{ m}$. Experimental results show that the accuracy of the two principles is acceptable.

4. ACCURACY LOSS ANALYSIS OF RDPC MODEL

The mapping relationship (9) can be approximated by the order- m polynomial, which is mentioned above. The first-order error transfer coefficient of the slant range r_2 can then be derived as follows [27]:

$$\frac{\partial \mathbf{P}}{\partial r_2} \approx -\frac{r_2}{B_{\perp} \cos \Phi_1} (\hat{\mathbf{P}} \times \hat{\mathbf{v}}) \quad (21)$$

where B_{\perp} is effective baseline, Φ_1 the angle included by \mathbf{P} and the cross-track plane, $\hat{\mathbf{P}}$ the unit vector of \mathbf{P} , and $\hat{\mathbf{v}}$ the satellite S_1 speed unit vector.

It is also possible to determine that:

$$\frac{\partial^2 \mathbf{P}}{\partial r_2^2} \approx -\frac{1}{B_{\perp} \cos \Phi_1} (\hat{\mathbf{P}} \times \hat{\mathbf{v}}) - \frac{r_2^2}{r_1 (B_{\perp} \cos \Phi_1)^2} [\hat{\mathbf{P}} - (\hat{\mathbf{P}} \cdot \hat{\mathbf{v}}) \hat{\mathbf{v}}] \quad (22)$$

$$\frac{\partial^3 \mathbf{P}}{\partial r_2^3} \approx -\frac{3r_2}{r_1 (B_{\perp} \cos \Phi_1)^2} [\hat{\mathbf{P}} - (\hat{\mathbf{P}} \cdot \hat{\mathbf{v}}) \hat{\mathbf{v}}] + \frac{r_2^3}{r_1^2 (B_{\perp} \cos \Phi_1)^3} (\hat{\mathbf{P}} \times \hat{\mathbf{v}}) \quad (23)$$

$$\frac{\partial^4 \mathbf{P}}{\partial r_2^4} \approx \frac{r_2^4 - 3r_1^2 (B_{\perp} \cos \Phi_1)^2}{r_1^3 (B_{\perp} \cos \Phi_1)^4} [\hat{\mathbf{P}} - (\hat{\mathbf{P}} \cdot \hat{\mathbf{v}}) \hat{\mathbf{v}}] \quad (24)$$

The error caused by use of the polynomial approximation can be analyzed as follows. According to the Taylor expansion remainder theorem, when the function $\mathbf{P}(\xi)$ is approximated by an order- m polynomial in the interval $[\xi_a, \xi_b]$ including ξ_i $i = \{0, 1, \dots, m\}$, $\zeta \in (\xi_a, \xi_b)$ exists s.t. the approximate error in point $\xi \in [\xi_a, \xi_b]$ is

$$E(\mathbf{P}(\xi); \xi) = \mathbf{P}(\xi) - \mathbf{P}_m(\xi) = \frac{\omega(\xi)}{(m + 1)!} \frac{\partial^{m+1}\mathbf{P}}{\partial \xi^{m+1}} \Big|_{\xi=\zeta} \quad (25)$$

where $\omega(\xi) = \prod_{i=0}^m (\xi - \xi_i)$.

Precisely determining $E(\mathbf{P}(\xi); \xi)$ is more complex; an upper limit on the error, a polynomial approximation in the worst case, can be expressed as:

$$E(\mathbf{P}(\xi); \xi) \leq \max \left(\frac{\omega(\xi)}{(m + 1)!} \right) \cdot \max \left(\frac{\partial^{m+1}\mathbf{P}}{\partial \xi^{m+1}} \Big|_{\xi=\zeta} \right) \quad (26)$$

For the three kinds of geolocation systems, accuracy analysis of the fast algorithm is described respectively as follows, which make use of polynomial approximation error equation.

In the case of InSAR, $\xi \triangleq \phi$, and $\phi = \frac{4\pi}{\lambda}(r_2 - r_1)$, and therefore:

$$\frac{\partial^k \mathbf{P}}{\partial \phi^k} = \left(\frac{\lambda}{4\pi} \right)^k \frac{\partial^k \mathbf{P}}{\partial r_2^k} \quad (27)$$

Substituting Equations (24) and (27) and the corresponding parameter ($B_{\perp} \approx 103$ m) of TerraSAR-X in Section 5 into Equation (26) and setting $m = 3$ for example gives:

$$E(\mathbf{P}(\phi); \phi) \leq \frac{|\phi_a - \phi_b|^4}{4!} \cdot \left(\frac{\lambda}{4\pi} \right)^4 \cdot \frac{r_2^4}{r_1^3(B_{\perp} \cos \Phi_1)^4} \leq \frac{|\phi_a - \phi_b|^4}{4!} \cdot 10^{-13} \quad (28)$$

where $|\hat{\mathbf{P}} \times \hat{\mathbf{v}}| \leq 1$ and $|\hat{\mathbf{P}} - (\hat{\mathbf{P}} \cdot \hat{\mathbf{v}}) \hat{\mathbf{v}}| \leq 1$ are used.

Assuming that $E(\mathbf{P}(\phi); \phi) \leq 0.01$, $|\phi_a - \phi_b| \leq 10^3$ is a conservative estimate from Equation (28), and this condition is easy to meet.

In the case of stereo SAR, $\xi \triangleq \Delta r$ and $\Delta r = r_2 - r_1$, and therefore:

$$\frac{\partial^k \mathbf{P}}{\partial \Delta r^k} = \frac{\partial^k \mathbf{P}}{\partial r_2^k} \quad (29)$$

Substituting Equations (24) and (29) and the corresponding parameter ($B_{\perp} \approx 175$ km) of TerraSAR-X in Section 5 into Equation (26) and taking $m = 3$ for example gives:

$$E(\mathbf{P}(\Delta r); \Delta r) \leq \frac{|\Delta r_a - \Delta r_b|^4}{4!} \cdot \frac{r_2^4}{r_1^3(B_{\perp} \cos \Phi_1)^4} \leq \frac{|\Delta r_a - \Delta r_b|^4}{4!} \cdot 10^{-15} \quad (30)$$

and this condition is also easily fulfilled. The baseline length of stereo SAR is much greater than that of InSAR, and therefore its polynomial approximation error is much less than that of InSAR.

In the case of single SAR geolocation, $\xi \triangleq h$. According to Equations (27) and (28), $h = r_2 - R_e$, and therefore:

$$\frac{\partial^k \mathbf{P}}{\partial h^k} = \frac{\partial^k \mathbf{P}}{\partial r_2^k} \quad (31)$$

Substituting Equations (23) and (31) and the corresponding parameter of TerraSAR-X in Section 5 into Equation (26) and taking $m = 2$ for example:

$$E(\mathbf{P}(h); h) \leq \frac{|h_a - h_b|^3}{3!} \cdot \frac{2r_2^3}{r_1^2(B_\perp \cos \Phi_1)^3} \leq \frac{|h_a - h_b|^3}{3!} \cdot 10^{-11} \quad (32)$$

This condition is also easy to achieve. The baseline length of single SAR is equal to the distance between the satellite and the center of the Earth, which is much greater than that of stereo SAR, and therefore its second-order polynomial approximation error is acceptable.

5. EXPERIMENTS AND RESULT ANALYSES

To test the effectiveness of this proposed fast geolocation method, it was used to process real data.

5.1. Experiments and Result Analyses for InSAR Geolocation

The data used are from the pairs of TerraSAR-X repeat-pass images obtained on April 23, 2008, and May 5, 2008. The effective baseline is equal to about 103 meters. The center position of the images is at latitude 39.52°N and longitude 96.55°E, which is the location of a mountain range in Gansu Province, China. A data size of 3200×2100 pixels was selected. The minimum elevation value is equal to 2250 meters, while the maximum elevation value is equal to 2872 meters. The data-processing results are shown in Figure 2.

Figure 2(a) shows the master SAR amplitude images for the selection region. The interferograms after processing (removal of flat-Earth phase, phase filtering and unwrapping) are shown in Figures 2(b), 2(c), and 2(d). The point-by-point DEM reconstruction results after the absolute interferometric phase was acquired are shown in Figure 2(e).

To evaluate algorithm performance for different sampling intervals, sampling intervals of azimuth (k) \times range (l) = $\{5 \times 5, 10 \times 10,$

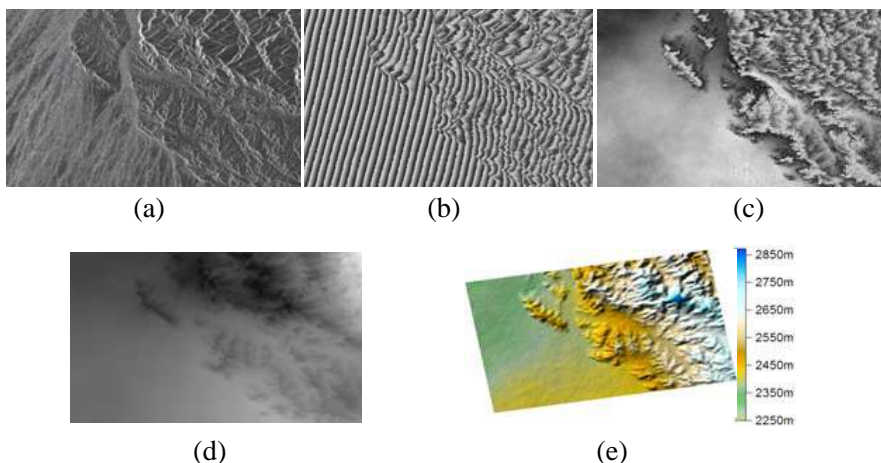


Figure 2. TerraSAR-X repeat-pass data-InSAR processing results. (a) TerraSAR-X SAR amplitude images. (b) Interferogram after the SAR image registration. (c) Interferogram after the removal of the flat-Earth phase. (d) Interferogram after phase filtering and unwrapping. (e) DEM reconstruction results obtained using the conventional point-by-point iterative method.

20×20 were used. Using the point-by-point InSAR geolocation result as a reference value, the fast InSAR geolocation performance for different sampling intervals is shown in Table 1. The geolocation was performed on a PC with an Intel Core2 Quad 2.33-GHz CPU and 2 GB memory and using the IDL programming language.

From Table 1, it can be seen that the computation time of the fast

Table 1. InSAR fast geolocation algorithm performance.

Sampling interval (pixels)	Runtime (s)	Mean square root of loss of precision (m)		
		X	Y	Z
*1 × 1	432	0	0	0
5 × 5	91	0.0134854	0.0061031	0.0091964
10 × 10	38	0.0296664	0.0137296	0.0203317
20 × 20	22	0.0808111	0.0377027	0.0554211
30 × 30	16	0.1865631	0.0713718	0.1258080

* 1 × 1 denotes no resampling, i.e., the point-by-point InSAR geolocation was applied.

algorithm decreases as the sampling interval increases, while the loss of precision also decreases. In practice, an appropriate sampling interval and an appropriate polynomial order would be selected according to the accuracy requirements or the computation time limits. For example, the loss of precision is difficult to accept for HRTI-3 standard which requires precision in meters when sampling interval is added to 30×30 . Thus, the maximum time savings for InSAR geolocation can be realized, while still meeting accuracy requirements.

From Table 1, it is evident that the actual loss of precision of InSAR geolocation is greater than the approximate cubic polynomial error obtained using the theoretical analysis presented in Section 4. There are two reasons for this. First, the previous theoretical analysis was based on the polynomial approximation error obtained using a Taylor expansion. However, in actual processing, the polynomial is obtained by fitting the data, so the approximation error is greater than that of a Taylor expansion. Second, the polynomials of the resampled coarse grid points are obtained by fitting, but the polynomials of most of the pixels were derived from the polynomial interpolation of the coarse grid points. This inevitably further degraded accuracy. Although the actual accuracy is lower than the theoretical accuracy, it still meets the requirements of the intended application.

5.2. Experiments and Result Analyses for Stereo SAR Geolocation

The data used are from the pairs of TerraSAR-X repeat-pass images obtained on November 28, 2008, and December 4, 2008. The effective baseline is equal to about 175 kilometers. The center position of the images is at latitude 47.18°N and longitude 7.69°E , which is the location of a mountain in Switzerland. A data size of 1500×1000 pixels was selected. The minimum elevation value is equal to 550 meters, while the maximum elevation value is equal to 821 meters. The data-processing results are shown in Figure 3.

Figures 3(a) and (b) show the master and slave SAR amplitude images for the selection region. The stereo SAR geolocation results obtained using the fast geolocation method are shown in Figure 3(c).

Similarly, using the point-by-point stereo SAR geolocation results as a reference value, the fast stereo SAR geolocation performance for different sampling intervals is shown in Table 2. These results also show that the fast algorithm has the advantages of high efficiency and constant accuracy. The fast algorithm efficiency is improved very limited when sampling interval is added to 50×50 . Comparing Table 1 with Table 2, it can be seen that in the same coarse sampling interval,

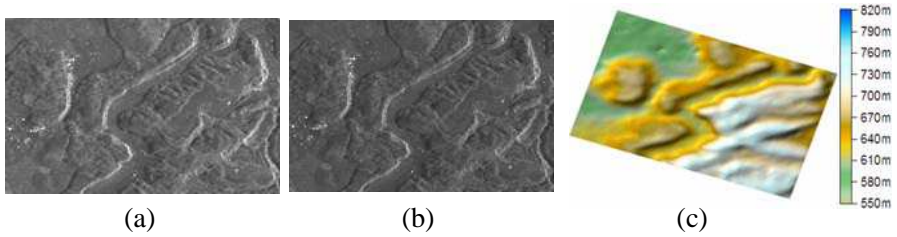


Figure 3. TerraSAR-X repeat-pass data-stereo SAR processing results. (a) TerraSAR-X SAR master amplitude images. (b) TerraSAR-X SAR slave amplitude images. (c) Stereo SAR geolocation results obtained using the fast geolocation method.

Table 2. Stereo SAR fast geolocation algorithm performance.

Sampling interval (pixels)	Runtime (s)	Mean square root of loss of precision (m)		
		X	Y	Z
* 1×1	294	0	0	0
5×5	57	0.0080212	0.0019805	0.0033649
10×10	21	0.0080283	0.0019822	0.0033679
20×20	13	0.0080425	0.0019858	0.0033739
50×50	12	0.0120953	0.0046485	0.0083915

* 1×1 denotes no resampling, i.e., the point-by-point stereo SAR geolocation was applied.

the stereo SAR fast algorithm error is smaller than that of InSAR, which is in good agreement with the analysis in Section 4.

5.3. Experiments and Result Analyses for Single SAR Geolocation

The data used are from TerraSAR-X SAR images obtained on April 23, 2008. The center position of the images is at latitude 39.28° and longitude 96.58° . The area consists of several ridges, and the average elevation is about 4190 meters. A data size of 4500×3500 pixels was selected. The data-processing results are shown in Figure 4. Figure 4(a) shows the SAR amplitude images. The chosen DEM data of SRTM is shown in Figure 4(b). The point-by-point results of single SAR geolocation is shown in Figure 4(c).

Similarly, using the point-by-point single SAR geolocation result as a reference value, the fast single SAR geolocation performance for

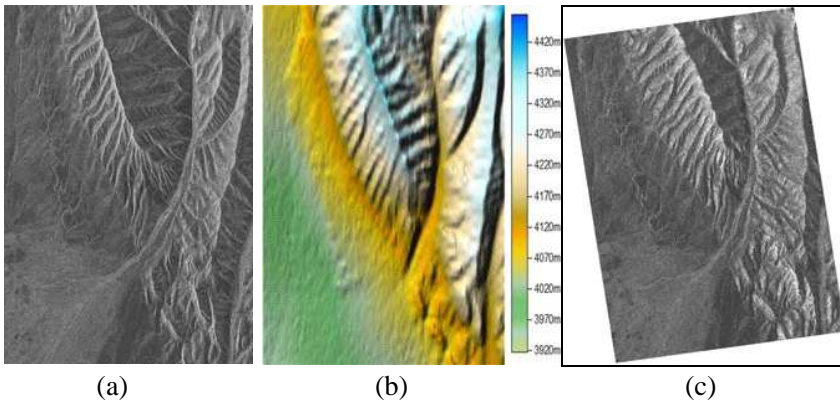


Figure 4. TerraSAR-X data-single SAR geolocation processing results. (a) TerraSAR-X SAR amplitude images. (b) DEM data of SRTM. (c) The point-by-point results of single SAR geolocation.

different sampling intervals is shown in Table 3. These results also show that the fast algorithm offers advantages of high efficiency and constant accuracy. The fast algorithm efficiency is improved very limited when sampling interval is added to 100×100 . Comparing Table 2 with Table 3, it is clear that in the same coarse sampling interval, the single SAR fast algorithm error is smaller than that of stereo SAR, which is in good agreement with the analysis presented in Section 4.

Table 3. Single SAR fast geolocation algorithm performance.

Sampling interval (pixels)	Runtime (s)	Mean square root of loss of precision (m)		
		X	Y	Z
* 1×1	1581	0	0	0
10×10	264	0.0002774	0.0000519	0.0002063
30×30	81	0.0002827	0.0000862	0.0002611
50×50	46	0.0003724	0.0001254	0.0003078
100×100	45	0.0012836	0.0008589	0.0009173

* 1×1 denotes no resampling, i.e., the point-by-point single SAR geolocation was applied.

In summary, experimental results for three kinds of systems show that the fast geolocation algorithm greatly reduces the amount of calculation required while maintaining high geolocation accuracy. Therefore, the effectiveness and correctness of the proposed method have been validated.

6. CONCLUSION

A unified fast solution for the single/interferometric/stereo SAR geolocation equations is proposed in this paper, which is based on the RDPC model. The fast algorithm using polynomial approximation solves the RD equation quickly and robustly, while the geolocation accuracy loss is small. For the three kinds of SAR geolocation system, geolocation equations represent the stable mapping relationship, which has no singularity and can be approximated by polynomials. The fast algorithm is general for the three cases. Loss on accuracy and speed of the algorithm must be a trade-off during actual use. In addition, accuracy of solution of the fast algorithm is also subject to the impact parameter errors, which is the same as that of RD method.

Several groups of TerraSAR-X measured data have been processed using the fast algorithm in the three cases. Experimental results show that the fast geolocation algorithm offers comprehensive advantages of high efficiency and constant accuracy. Compared with the point-by-point iterative algorithm, for the case of single SAR image geolocation, the fast algorithm efficiency is improved by approximately 40 times, and the loss of precision is in the 10^{-4} order of magnitude. In the case of stereo SAR geolocation, the fast algorithm efficiency is improved by approximately 20 times, and the loss of precision is close to 10^{-2} m. In the case of InSAR geolocation, the fast algorithm efficiency is improved by approximately 20 times, and the loss of precision is close to 10^{-1} m. The loss of precision can be accepted for HRTI-3 standard that requires precision in meters. Therefore this method for SAR global observation data processing can play an important role in further SAR research. Future studies will address fast-algorithm efficiency, further enhancements, more in-depth error analysis, and other topics.

ACKNOWLEDGMENT

This work was supported by the National Natural Science Foundation of China (Grant No. 61002031). The authors wish to thank the German Aerospace Center (DLR) and the Infoterra Company for providing the TerraSAR-X data.

REFERENCES

1. Li, S., H. P. Xu, and L. Q. Zhang, "An advanced DSS-SAR InSAR terrain height estimation approach based on baseline decoupling," *Progress In Electromagnetics Research*, Vol. 119, 207–224, 2011.

2. An, D.-X., Z.-M. Zhou, X.-T. Huang, and T. Jin, "A novel imaging approach for high resolution squinted spotlight SAR based on the deramping-based technique and azimuth NLCS principle," *Progress In Electromagnetics Research*, Vol. 123, 485–508, 2012.
3. Chen, J., S. Quegan, and X. J. Yin, "Calibration of spaceborne linearly polarized low frequency SAR using polarimetric selective radar calibrators," *Progress In Electromagnetics Research*, Vol. 114, 89–111, 2011.
4. Leberl, F., "Radargrammetry for image interpretation," ITC Technical Report, 1978.
5. Krieger, G., A. Moreira, H. Fiedler, et al., "TanDEM-X: A satellite formation for high-resolution SAR interferometry," *IEEE Transactions on Geoscience and Remote Sensing*, Vol. 45, 3317–3341, 2007.
6. Chen, P. H. and I. J. Dowman, "A weighted least square solution for space intersection of spaceborne stereo SAR data," *IEEE Transactions on Geoscience and Remote Sensing*, Vol. 39, 233–240, 2001.
7. Collino, F., F. Millot, and S. Pernet, "Boundary-integral methods for iterative solution of scattering problems with variable impedance surface condition," *Progress In Electromagnetics Research*, Vol. 80, 1–28, 2008.
8. Ma, L., Z. F. Li, and G. S. Liao, "System error analysis and calibration methods for multi-channel SAR," *Progress In Electromagnetics Research*, Vol. 112, 309–327, 2011.
9. Zhang, Y.-J., H.-F. Huang, Y.-S. Zhang, and D.-N. Liang, "InSAR error modeling and error estimation method," *Acta Electronica Sinica*, Vol. 39, No. 6, 2011.
10. Krieger, G., M. Zink, H. Fiedler, et al., "The TanDEM-X mission: Overview and status," *IEEE Radar Conference*, 372–376, 2009.
11. Leberl, F., *Radargrammetric Image Processing*, Artech House, Norwood, Massachusetts, 1990.
12. Bolter, R. and F. Leberl, "Fusion of multiple view interferometric and slant range SAR data for building reconstruction," *SAR Image Analysis, Modelling, and Techniques III, SPIE Proceedings Series*, Vol. 4173, 241–250, F. Posa and L. Guerriero, Eds., Barcelona, Spain, Sep. 25–27, 2000.
13. Konecny, G. and W. Schuhu, "Reliability of radar image data," *16th ISPRS Congress*, B9, Tokyo, 1988.
14. Fraser, C. S. and H. B. Hanley, "Bias compensation in rational functions for Ikonos satellite imagery," *Photogrammetric*

- Engineering & Remote Sensing*, Vol. 69, No. 1, 53–57, 2003.
15. Zhang, G., W. B. Fei, Z. Li, X. Y. Zhu, and D. R. Li, “Evaluation of the RPC model for spaceborne SAR imagery,” *Photogrammetric Engineering & Remote Sensing*, Vol. 76, 727–733, 2010.
 16. Brown, W. E., “Applications of SEASAT SAR digitally correlated imagery for sea ice dynamics,” *Amer. Geophys. Union Spring Meeting*, 25–29, 1981.
 17. Curlander, J. C., “Location of spaceborne SAR imagery,” *IEEE Trans. on Geoscience and Remote Sensing*, Vol. 20, No. 3, 359–364, 1982.
 18. Yuan, X., *Introduce to the Spaceborne Synthetic Aperture Radar*, National Defense Industry Press, Beijing, 2003 (in Chinese).
 19. Li, F. K. and W. T. Johoson, “Ambiguities in spaceborne synthetic aperture radar systems,” *IEEE Transactions on Geoscience and Remote Sensing*, 389–396, 1983.
 20. Roth, A., D. Kosmann, M. Matschke, et al., “Experiences in multi-sensorial SAR geocoding,” *IGARSS 1996*, 27–31, 1996.
 21. Liu, X. K., H. Ma, and W. Sun, “Study on the geolocation algorithm of space-borne SAR image,” *IWICPAS 2006*, 270–280, 2006.
 22. Raggam, H., K. Gutjahr, R. Perko, and M. Schardt, “Assessment of the stereo-radargrammetric mapping potential of TerraSAR-X multibeam spotlight data,” *IEEE Transactions on Geoscience and Remote Sensing*, Vol. 48, No. 2, 971–977, 2010.
 23. Rodriguez, E. and M. J. Martin, “Theory and design of interferometric synthetic aperture radar,” *IEE Proc.*, Vol. 139, No. 2, 147–159, 1992.
 24. Goblirsch, W., “The exact solution of imaging equations for crosstrack interferometers,” *Proceedings of the 1997 IEEE International Geoscience and Remote Sensing Symposium*, Vol. 1, 439–441, Aug. 3, 1997.
 25. Zheng, X., K. Wang, and X. Liu, “A new DEM reconstruction method based on an accurate flattening algorithm in interferometric SAR,” *IEEE International Conference on Acoustics, Speech and Signal Processing, ICASSP*, 1093–1096, Mar. 31, 2008.
 26. Giovanni, N., “Exact closed-form geolocation for SAR interferometry,” *IEEE Transactions on Geoscience and Remote Sensing*, Vol. 40, 220–222, 2002.
 27. Eugenio, S., “A simple and exact solution for the interferometric and stereo SAR geolocation problem,” *IEEE Transactions on Geoscience and Remote Sensing*, Vol. 42, 1625–1634, 2004.

28. Rossi, C., M. Eineder, T. Fritz, and H. Breit, "TanDEM-X mission: Raw DEM generation," *EUSAR 2010*, 146–149, 2010.
29. Schwabisch, M., "A fast and efficient technique for SAR interferogram geocoding," *Proceedings of the 1998 IEEE International Geoscience and Remote Sensing Symposium*, 1100–1102, 1998.
30. Eineder, M., "Efficient simulation of SAR interferograms of large areas and of rugged terrain," *IEEE Transactions on Geoscience and Remote Sensing*, Vol. 41, No. 6, Part 1, 1415–1427, 2003.